

A DNA Methylation Network Interaction Measure, and Detection of Network Oncomarkers

Thomas E. Bartlett^{1,3*}, Sofia C. Olhede^{2,3}, Alexey Zaikin¹

1 Department of Mathematics, University College London, London, United Kingdom, **2** Department of Statistical Science, University College London, London, United Kingdom, **3** CoMPLEX, University College London, London, United Kingdom

Abstract

Epigenetic processes—including DNA methylation—are increasingly seen as having a fundamental role in chronic diseases like cancer. DNA methylation patterns offer a route to develop prognostic measures based directly on DNA measurements, rather than less-stable RNA measurements. A novel DNA methylation-based measure of the co-ordinated interactive behaviour of genes is developed, in a network context. It is shown that this measure reflects well the co-regulatory behaviour linked to gene expression (at the mRNA level) over the same network interactions. This measure, defined for pairs of genes in a single patient/sample, associates with overall survival outcome independent of known prognostic clinical features, in several independent data sets relating to different cancer types. In total, more than half a billion CpGs in over 1600 samples, taken from nine different cancer entities, are analysed. It is found that groups of gene-pair interactions which associate significantly with survival identify statistically significant subnetwork modules. Many of these subnetwork modules are shown to be biologically relevant by strong correlation with pre-defined gene sets, such as immune function, wound healing, mitochondrial function and MAP-kinase signalling. In particular, the wound healing module corresponds to an increase in co-ordinated interactive behaviour between genes for worse prognosis, and the immune module corresponds to a decrease in co-ordinated interactive behaviour between genes for worse prognosis. This measure has great potential for defining DNA-based cancer biomarkers. Such biomarkers could naturally be developed further, by drawing on the rapidly expanding knowledge base of network science.

Citation: Bartlett TE, Olhede SC, Zaikin A (2014) A DNA Methylation Network Interaction Measure, and Detection of Network Oncomarkers. *PLoS ONE* 9(1): e84573. doi:10.1371/journal.pone.0084573

Editor: Zoran Culig, Innsbruck Medical University, Austria

Received: September 17, 2013; **Accepted:** November 24, 2013; **Published:** January 6, 2014

Copyright: © 2014 Bartlett et al. This is an open-access article distributed under the terms of the Creative Commons Attribution License, which permits unrestricted use, distribution, and reproduction in any medium, provided the original author and source are credited.

Funding: This work was funded via UCL CoMPLEX, by the Medical Research Council and the Engineering and Physical Sciences Research Council (EPSRC). SCO acknowledges funding from EPSRC grant no. EP/I005250/1. AZ acknowledges financial support from CR-UK and Eve Appeal (PROMISE-2016). The funders had no role in study design, data collection and analysis, decision to publish, or preparation of the manuscript.

Competing Interests: The authors have declared that no competing interests exist.

* E-mail: thomas.bartlett.10@ucl.ac.uk

Introduction

Epigenetic information is stored in the genome in the form of heritable modifications to the chemical structure of DNA, such as methylation of CpG di-nucleotides. Epigenetic information can be modulated during the lifetime of an organism by environmental cues [1–3] and these changes persist in subsequent mitoses, leading to an acquired change of phenotype. As such, epigenetics can be considered to be an interface between the genome and the environment, and consequently also a conduit for environmental risk factors.

Alterations in DNA methylation (DNAm) levels are among the earliest changes in human carcinogenesis [1], and hence offer novel strategies to identify individuals who might be at risk of developing such illnesses or individuals with early stage cancers. However, to proceed with developing such tests, measures relating to DNA methylation are needed, which can be consistently linked to clinically relevant differences, such as patient outcome. Per-gene measures of DNA methylation have been shown to be relevant to the study of cancer genomics [4], and network models and measures naturally reflect the collective behaviour of groups of similar items, such as genes, and their interactions with one another. As such, they may help with the development of DNAm-

based biomarkers which take account of such collective and interactive behaviour of genes.

As a cancer progresses, its signalling and control networks are re-arranged ('re-wired'), and this drives adaptive alterations in phenotype, which are advantageous for the cancer [5]. Previous research by other authors [6] found that patient survival outcome in breast cancer (BRCA) could be predicted well by network models of this re-wiring, based on gene expression data. DNAm patterns are more stable than gene expression patterns, because DNAm measurements are taken directly from DNA, whereas gene expression measurements must come via RNA. Hence, DNAm patterns might be expected to lead to more reliable disease biomarkers than gene expression patterns would be able to. Here, we develop a measure of network interaction 'co-ordinatedness', between pairs of genes, based on DNA methylation data. We show that this measure, calculated for pairs of genes, is highly associated with co-regulatory behaviour linked to gene expression (at the mRNA level) over the same network interactions/pairs of genes. We show that this measure associates significantly with overall survival outcome independent of known prognostic markers in several data sets and cancer types, and that groups of these significant gene-gene network interactions identify subnetwork modules, with a well-controlled false discovery rate. Of these significant subnetwork modules, one module corresponds very

strongly to wound healing, with its gene-gene interactions displaying an increase in co-ordinated behaviour with worse disease prognosis. Another of these significant subnetwork modules corresponds very strongly to immune function, with its gene-gene interactions predominantly showing a decrease in co-ordinated behaviour with worse disease prognosis. Our findings provide the basis for further development of independent DNA methylation oncomarkers in the context of network science.

Results

The DNA Methylation Network Correlation Measure

The DNA methylation (DNAm) network correlation measure quantifies the extent to which the DNA methylation profiles of a pair of genes ‘explain’ each other. It is based only on measurements of the DNA methylation profiles of this pair of genes, and it acts as a surrogate for a measure of the extent to which this pair of genes behave interactively. Such interactive behaviour may include transcriptional regulation or other types of biochemical interaction, and a pair of genes will affect each other’s transcriptional behaviour or other biochemical functioning most directly as a result of their own expression levels. An increase in methylation level around the gene promoter is certainly correlated with a decrease in the expression level of the gene, although which of these occurs first is not clear [7]. An increase in methylation level in the gene body is related less certainly to effects on gene transcriptional and translational behaviour, which may include increased expression level and alternatively spliced gene products [7]. Hence, there may be a number of components of the variation of the methylation profile of a gene which are significant in terms of their correlation with different transcriptional effects of that gene. The methylation profile of a gene is taken as a surrogate for these various interactive effects in the DNAm network cross correlation measure, which quantifies the extent to which these interactive effects or patterns in a pair of genes explain each other, as reflected in the DNA methylation profiles.

The DNAm network cross correlation measure is defined by analogy to Canonical Correlation Analysis (CCA) [8] (see ‘methods and models’ for formal definitions). CCA aims to discover linear combinations of variables of one type, and linear combinations of variables of another type, so that these combinations best ‘explain’ each other. In this context, a particular way of combining (by scaling and adding) the deviations from the mean methylation profile at a number of locations within one gene might be particularly effective at explaining a particular combination (again, by scaling and adding) of the deviations from the mean methylation profile at a number of locations in another gene, and *vice-versa*. There will probably be fewer ways in which the methylation levels of these genes vary across the samples, than there are locations at which methylation is measured, along each gene; this is because the methylation level at many locations along a gene is highly correlated. CCA finds the most important components of this variation across samples (in terms of these linear combinations of variables of each type, i.e., methylation measurements in each gene) which both these types of variables (i.e., DNA methylation in the two genes considered) have in common.

CCA finds linear combinations of the two types of variables that covary. Because linear combinations are evaluated, the two types of variables can be of a different number. The DNAm network cross correlation measure therefore evaluates the extent to which, in an individual sample, these combinations in this pair of types of variables explain each other. The covariation is assessed against typical variability in such variables. Such variation is assessed in

terms of the evaluated statistics. Variation is understood in terms of the population covariance matrix, inherent to healthy samples, the methylation profile for one gene makes up the variables of one type, and the variables of that type are the methylation points, i.e., CpGs, along that gene. There are many sources of variation. When the DNAm network cross correlation measure is large (i.e., close to 1), the corresponding pair of genes explain each others transcriptional or translational behaviour (as reflected in their methylation profiles) well, or have otherwise well-correlated interactive behaviour, for the corresponding sample (patient); see figure 1.

Application of the DNA Methylation Network Correlation Measure to Data

The DNAm network correlation measure was developed and evaluated in the context of DNAm data obtained via the Illumina Infinium Human Methylation 450 K platform, from samples from cancer patients made publicly available via The Cancer Genome Atlas (TCGA) project [9–11], relating to nine different cancer types. Details of the number of samples (patients) for which DNA methylation and survival analysis were carried out, for each data set, appear in table 1.

For each data set, considering all possible pairs of the 14800 genes available would require more than 10^8 comparisons, each based on the data for a pair of genes across all the samples in that data set. Further, it is possible that spurious correlations could arise if all possible pairs of genes were considered in this way. For example, the expression and regulatory patterns of a pair of genes may be highly correlated if they are both part of the same signalling pathway, even if they do not directly interact. To avoid problems due to the high number of tests inherent to considering all pairwise gene interactions, we restricted the number of pairs of genes for which the DNAm network correlation measure was considered. The DNAm network correlation measure was only calculated for a pair of genes, and subsequent analyses were only carried out, if that pair of genes was listed as taking part in a known biochemical interaction. We note that [6] proposed such a restriction for pairwise gene interactions, and applied it successfully. A list of such interactions was downloaded from <http://www.pathwaycommons.org>, and was used as a canonical human interactome map.

Comparing the DNA Methylation Network Correlation Measure with Gene Expression Network Correlation

In order to test whether a major component of the interactive/co-regulatory behaviour quantified by the DNA methylation network correlation measure corresponds to that which can be measured by mRNA levels, the following procedure was carried out. For the five data sets included in the subsequent DNA methylation analysis for which sufficient gene expression data (in the form of mRNA levels) were available, for each pair of genes for which the DNAm network correlation measure was calculated, the Spearman correlation coefficient of the mRNA expression levels for that pair of genes was calculated, across all the cancer samples with gene expression data available for that tumour type. For each of these pairs of genes, the mean of the DNA methylation network correlation measure was also calculated across all available (cancer) samples. The significance of association of the mean DNAm network correlation measure with the mRNA expression (gene expression) network correlation coefficient across all pairs of genes is shown in table 2, for each data set. Note that table 2 shows different numbers of samples for each cancer type to table 1, because the DNA methylation and gene expression analyses were

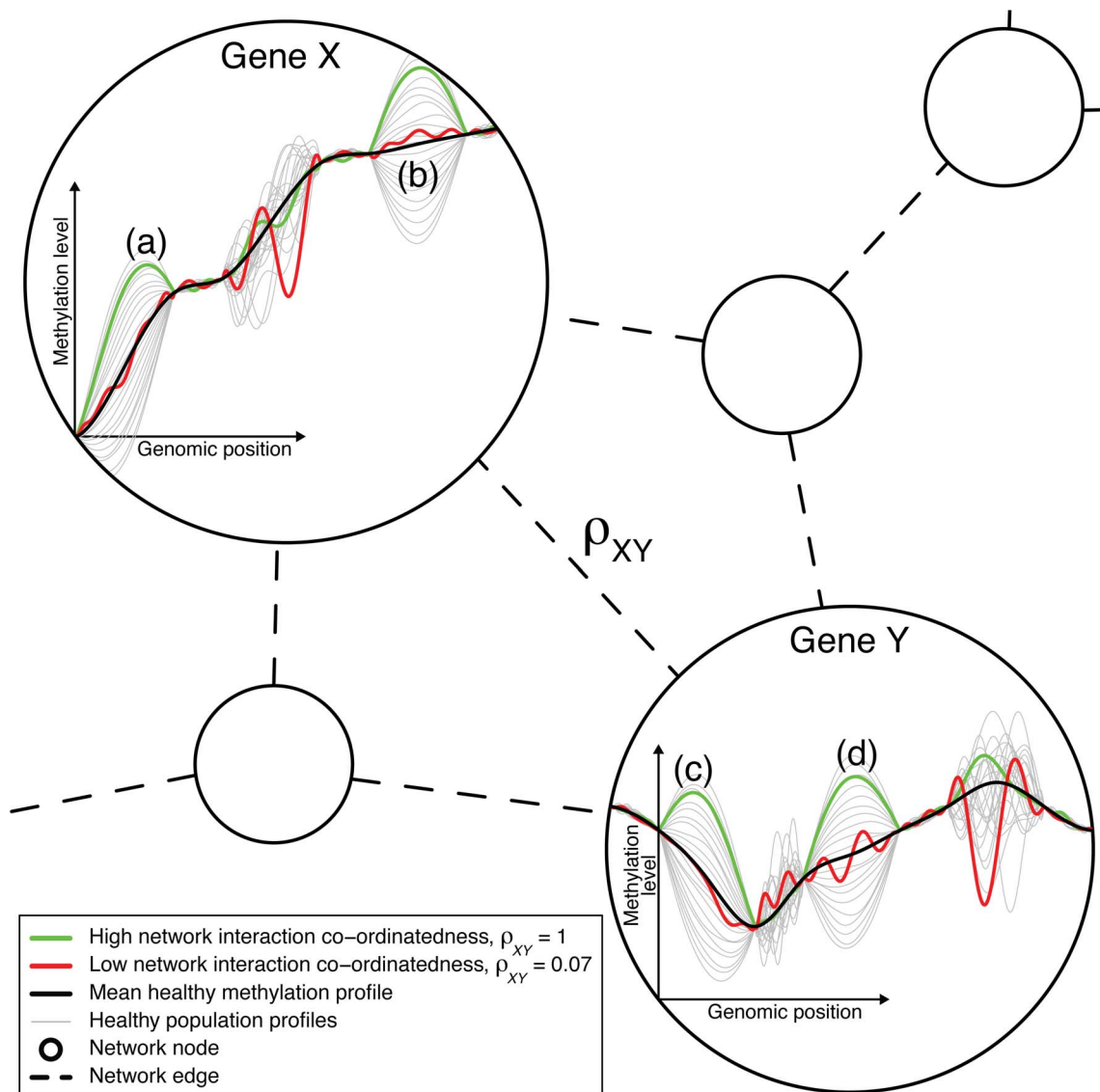


Figure 1. The DNA methylation network interaction measure. A combination of the variation of the healthy methylation profiles in regions (a) and (b) of gene X explains well/is well-explained by a combination of the variation of the healthy methylation profiles in regions (c) and (d) of gene Y. The green cancer sample varies by a large amount about the mean methylation profile and in a typical way in these regions in both genes. Hence, the green sample corresponds to a high level of network interaction co-ordinatedness, as measured by the DNA methylation network interaction measure, $\rho_{XY} = 1$. The variation in the other regions of these genes do not well-explain each other, and so the red sample, which varies by a large amount in these other regions and varies less and in an atypical way in regions (a)–(d), corresponds to a low level of network interaction co-ordinatedness, $\rho_{XY} = 0.07$. Genes X and Y are likely to have different numbers of methylation measurement locations (i.e., variables X and Y are of different dimension). The ordering of the measurement locations has no influence on the calculation of ρ , as long as the ordering is consistent across samples.

doi:10.1371/journal.pone.0084573.g001

based mostly on different samples from the same cancer type. Absolute values of these correlation measures are compared, because negative values mean different things in relation to the DNAm network correlation measure, and to the correlation coefficient of the gene expression data. For each data set, a Spearman correlation test comparing these network correlation measures across all pairs of genes is very significant, with $p \leq 2.3 \times 10^{-17}$ for all five data sets considered. Hence, it is concluded that a major component of the interactive behaviour quantified by the DNAm network correlation measure is the interactive (co-regulatory) behaviour corresponding to gene expression, at the mRNA level.

In many (approximately one third) of gene-pair comparisons made by the DNAm network correlation measure, it was calculated that there are two or more significant components of covariation between these pairs of genes, as determined by examining the corresponding cross-covariance matrices. Each such calculation was carried out by performing a singular value decomposition to estimate the variances corresponding to the main components of variation, and comparing these to empirical null model variances calculated similarly after randomising the original data, as in previous genomics studies by other authors [12]. The most likely candidates for these additional components of covariation which are measured by the DNAm network

Table 1. Number of samples in each data set.

| | Samples | Events |
|------|---------|--------|
| BLCA | 108 | 31 |
| BRCA | 173 | 23 |
| COAD | 237 | 36 |
| HNSC | 266 | 89 |
| KIRC | 265 | 91 |
| LIHC | 50 | 20 |
| LUAD | 143 | 45 |
| LUSC | 141 | 48 |
| UCEC | 276 | 28 |

Number of samples (patients) in each data set, together with number of events (i.e., number of patients who died before the end of the respective study). Abbreviations as follows: Bladder Urothelial Carcinoma (BLCA), Breast Invasive Carcinoma (BRCA), Colon Adenocarcinoma (COAD), Head and Neck Squamous Cell Carcinoma (HNSC), Kidney Renal Clear Cell Carcinoma (KIRC), Kidney Renal Papillary Cell Carcinoma (KIRP), Liver (LIHC), Lung Adenocarcinoma (LUAD), Lung Squamous Cell Carcinoma (LUSC), and Uterine Corpus Endometrioid Carcinoma (UCEC).

doi:10.1371/journal.pone.0084573.t001

correlation measure, beyond gene expression, include other components of biochemical interactive behaviour such as those associated with alternatively spliced forms of the gene product (such as alternatively spliced forms are thought to be linked to DNA methylation, [7]). However, it is not possible to test these hypotheses further using the publicly available data analysed here. A further study, involving collection of additional data such as RNA-seq or other transcriptome-level data collected with DNA methylation data, would have the potential for investigating such additional possibilities.

Association of the DNAm Network Correlation Measure with Patient Survival Outcome

The DNA methylation network correlation measure was tested against patient survival outcome, and further methodology was developed in this context, in order to develop the DNAm network correlation measure as a basis for prognostic biomarkers. For each data set, for each pair of genes, the association of the DNAm network correlation measure with patient overall survival outcome was tested by Cox regression, adjusted for clinical covariates. This adjustment for clinical covariates was carried out in order to develop a novel prognostic measure which is independent of known prognostic clinical features, such as age, disease stage and grade, and to take account of possible confounding (see 'methods and models' for further details). Heatmaps showing p -values of association of the DNAm network correlation measure with patient survival outcome, for the BRCA data set, for all interactions and for just those which appear in the canonical human interactome map, appear in figure S1, together with equivalent heatmaps produced from randomly generated p -values, to show the structure in this network model provided by the canonical human interactome map.

The canonical human interactome map defines 276136 interactions for the 8614 genes which are also present in each of the data sets considered here. For each of the 9 data sets, the 276136 p -values resulting from the tests of association with patient overall survival outcome (adjusted for clinical covariates) for each of these interactions are plotted in histograms, which appear in figure 2. For the COAD and LIHC data sets there is no

Table 2. Significance of association of the DNAm network correlation measure with gene expression network correlation.

| Data set | Samples | p -value |
|----------|---------|-----------------------|
| BRCA | 590 | 4.4×10^{-19} |
| COAD | 174 | 5×10^{-21} |
| KIRC | 72 | 3.2×10^{-17} |
| LUSC | 155 | 6×10^{-38} |
| UCEC | 54 | 2.3×10^{-17} |

For each gene-pair for which the DNAm network correlation measure is calculated, for which there are also mRNA expression (gene expression) data available, the Spearman correlation coefficient comparing the expression levels of that pair of genes is calculated across the available samples in a given data set (tumour samples only). For each pair of genes, the mean of the DNAm network correlation measure across the available samples in that data set is also calculated. These mean DNAm network correlation and expression network correlation measures are compared across all pairs of genes for each data set, with the corresponding p -values (Spearman correlation test) shown in the table. doi:10.1371/journal.pone.0084573.t002

association with survival. However for the other seven data sets (cancer types), and in particular BRCA, KIRC, LUAD, LUSC and UCEC, the concentration of p -values close to $p = 0$ shows that there are many pairs of genes for which the DNAm network correlation measure associates significantly with survival. It is important to note that the poor correlation for certain data sets is strongly linked, as would be expected, to the size of the data sets, and in particular to the number of events in the data sets (table 1). Applying these methods to larger data sets will be necessary for the development and validation of robust biomarkers.

Identification of Significant and Biologically Relevant Subnetworks

The data sets for which the DNAm network correlation measure did not show a correlation with survival outcome, COAD and LIHC, were excluded from the subsequent analyses, which proceeded with the seven remaining data sets, BLCA, BRCA, HNSC, KIRC, LUAD, LUSC and UCEC. If genes represent network nodes, significant subnetworks, modules, or motifs can be derived from the canonical human interactome map, by retaining the network edges (i.e., pairwise interactions between genes) which correspond to the DNAm network correlation measures which associate significantly with patient overall survival outcome. A significant subnetwork, module, or motif is then made up of genes which are connected by edges which are significantly associated with survival outcome. Some genes are connected to a large number of other genes in the canonical interactome map (i.e., they have high degree). If edges are defined as significant when they correspond to $p < 0.05$ of association with patient survival outcome, then a node (gene) of high degree would be expected to be connected to some other genes by significant edges which are in fact false positives. If several nodes of high degree are connected together by false positives in this way, it would result in a subnetwork being falsely declared significant; this could happen anywhere in the canonical interactome map where several high-degree nodes are connected together. To mitigate this effect, for each node (gene), the p -values of association with survival outcome for each of its connected edges (interactions) were converted to FDR (false discovery rate) adjusted q -values [13] with respect to that node (gene). Each edge (interaction) was then only marked as significant if it associated significantly with patient survival

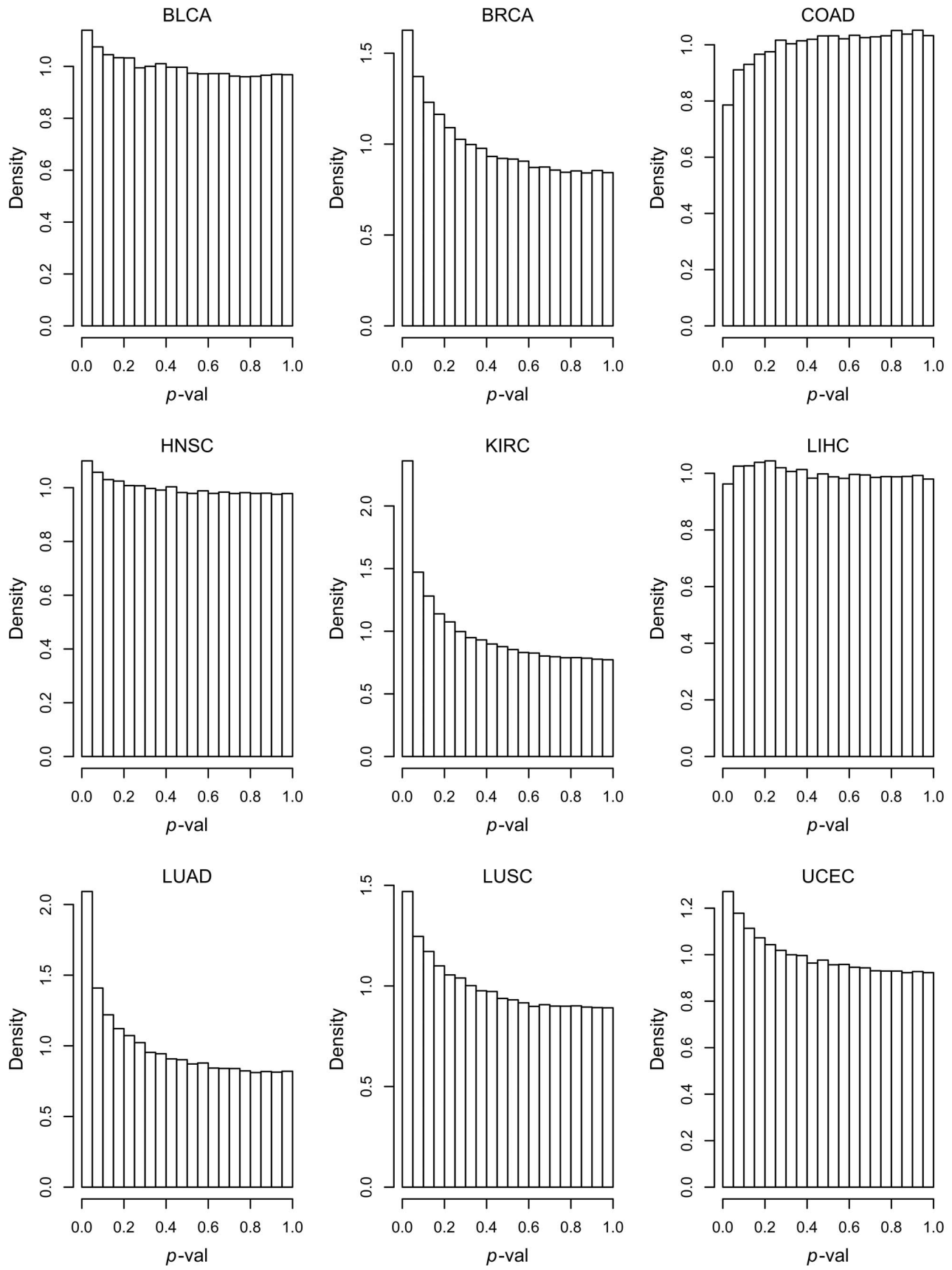


Figure 2. *p*-value histograms, showing the association of the DNA methylation network correlation measure with patient overall survival outcome, for all data sets. For each network edge, which connects a pair of genes (nodes), Cox regression is used to calculate a *p*-value

(adjusted for clinical covariates), which represents the association of the DNAm network correlation measure for that edge with patient survival outcome. For COAD and LIHC, there is no association of the DNAm network correlation measure with patient outcome. For the other data sets (cancer types), and in particular BRCA, KIRC, LUAD, LUSC and UCEC, the collection of *p*-values close to 0 shows that, for those data sets, the DNAm network correlation measure for many network edges is associated with patient outcome.
doi:10.1371/journal.pone.0084573.g002

outcome with $q < 0.05$ according to both the nodes (genes) connected by that edge.

Significant subnetworks, modules, and motifs found in this way were tested for biological relevance, by checking the genes comprising each subnetwork using gene set enrichment analysis (GSEA) [14]. For each significant subnetwork, module or motif, 6811 gene set definitions, downloaded from the Broad Institute Molecular Signatures Database (<http://www.broadinstitute.org>), were tested one by one for enrichment by the genes which comprise the respective subnetwork, module, or motif; further details about these gene sets can be found at that website. These enrichment tests were carried out using a one-sided Fisher's exact test, and if any of the 6811 gene sets showed significant enrichment ($q < 0.05$) by the genes comprising a subnetwork, module, or motif, it was marked as having biological relevance, according to the findings of previous work. The numbers of significant subnetworks, modules and motifs, arranged according to number of genes/nodes, and the numbers of these found to be biologically relevant, appear in table 3.

To check how well this methodology guards against falsely declaring subnetworks as significant, exactly the same process of significant subnetwork identification was applied to *p*-values randomly generated by sampling from a uniform(0,1) distribution and assigned to the 276136 interactions, and this process was

repeated 10^4 times. Table 4 shows the number of null subnetworks produced, of each size, in total over the 10^4 iterations. If there were no association of the DNAm network correlation measure with survival outcome (which would correspond to uniformly distributed *p*-values across these features), the expected number of 3-node subnetworks falsely declared as significant in a particular data set would be 4.0, the expected number of falsely identified 4-node subnetworks would be 0.34, and for 5 nodes the expected number would be 0.037. Comparison of these numbers with table 3 and the definition of the false discovery rate implies (taking into account these seven data sets) $FDR \leq 1$ for 3 node subnetworks, $FDR \leq 0.34$ for 4 node subnetworks, and $FDR \leq 0.037$ for 5 node subnetworks. Further, no individual gene appeared in these null subnetworks with at least 5 nodes more than twice out of the 10^4 iterations. As these small motifs of 3 and 4 nodes are of less interest in general, and because by excluding them the subnetwork false discovery rate is well-controlled, in the subsequent analysis, only subnetworks, modules and motifs with at least 5 nodes were considered as significant.

A network edge which is significant due to a correlation between a higher value of the DNAm network correlation measure and worse patient survival time (i.e., hazard ratio, $HR > 1$), corresponds to an increasing tendency of the genes (nodes) at either end of this network edge to explain each other's regulatory behaviour, the worse the prognosis of the cancer. This can be thought of as an increase in network interaction 'co-ordinatedness' between these genes corresponding to worse disease prognosis, or a 'positive network re-wiring' that is adaptively advantageous for the cancer. The opposite effect, where a network edge is significant due to a correlation between a lower value of the DNAm network correlation measure and worse patient survival time (i.e., hazard ratio, $HR < 1$), is equivalent to a decrease in network interaction co-ordinatedness for worse disease prognosis, or 'negative network re-wiring'. The proportion of significant network edges with $HR > 1$ (increase in network interaction co-ordinatedness for worse disease prognosis) is shown for each data set in table 5.

Table 3. Number of significant subnetworks, modules and motifs.

| Nodes | BLCA | BRCA | HNSC | KIRC | LUAD | LUSC | UCEC |
|-------|--------------|--------------|-------|--------------|--------------|--------------|--------------|
| 3 | 4 (1) | 19 (8) | 9 (5) | 19 (6) | 38 (10) | 11 (2) | 8 (1) |
| 4 | 1 (0) | 9 (3) | 2 (0) | 9 (3) | 12 (6) | 5 (1) | 5 (1) |
| 5 | 2 (2) | 1 (1) | 1 (0) | 1 (0) | 5 (1) | 0 (0) | 4 (1) |
| 6 | 1 (0) | 1 (0) | 1 (0) | 1 (0) | 2 (0) | 1 (0) | 2 (2) |
| 7 | 0 (0) | 1 (0) | 1 (0) | 1 (1) | 2 (0) | 0 (0) | 0 (0) |
| 8 | 0 (0) | 0 (0) | 0 (0) | 1 (1) | 2 (0) | 0 (0) | 1 (1) |
| 9 | 1 (1) | 1 (0) | 0 (0) | 2 (0) | 1 (1) | 1 (0) | 0 (0) |
| 10 | 0 (0) | 0 (0) | 0 (0) | 0 (0) | 0 (0) | 1 (0) | 0 (0) |
| 11 | 0 (0) | 0 (0) | 1 (0) | 0 (0) | 1 (1) | 0 (0) | 2 (1) |
| 13 | 0 (0) | 0 (0) | 0 (0) | 0 (0) | 1 (1) | 0 (0) | 0 (0) |
| 14 | 0 (0) | 0 (0) | 0 (0) | 0 (0) | 0 (0) | 1 (0) | 0 (0) |
| 16 | 0 (0) | 0 (0) | 0 (0) | 0 (0) | 0 (0) | 1 (0) | 0 (0) |
| 17 | 1 (0) | 0 (0) | 0 (0) | 0 (0) | 0 (0) | 0 (0) | 0 (0) |
| 18 | 0 (0) | 0 (0) | 0 (0) | 0 (0) | 0 (0) | 1 (1) | 0 (0) |
| 24 | 1 (0) | 0 (0) | 0 (0) | 0 (0) | 0 (0) | 0 (0) | 0 (0) |
| 27 | 0 (0) | 0 (0) | 1 (0) | 0 (0) | 0 (0) | 0 (0) | 0 (0) |
| 373 | 0 (0) | 0 (0) | 0 (0) | 0 (0) | 1 (1) | 0 (0) | 0 (0) |
| 770 | 0 (0) | 0 (0) | 0 (0) | 1 (1) | 0 (0) | 0 (0) | 0 (0) |

The number of significant subnetworks, modules and motifs found with each number of nodes (genes) is shown for each data set. Of these, the numbers found to have biological relevance (as determined by gene set enrichment analysis) are shown in brackets. Modules and larger subnetworks subsequently plotted in figures 3 and 4 are shown in bold.

doi:10.1371/journal.pone.0084573.t003

Smaller Significant and Biologically Relevant Network Modules of Interest

Detailed consideration of the smaller network modules identified as significant, and biologically relevant, confirms their relevance to cancer biology. Amongst the gene sets significantly enriched by the significant network modules, as well as numerous specific cancer gene sets, gene sets appear multiple times relating to JAK-STAT signalling, WNT signalling, GPCR signalling, EGFR signalling, VEGF signalling, interleukin activity, neutrophil activity/response to wounding, immune activity, metabolic activity/TCA cycle/mitochondria, chromosome maintenance, developmental processes/stem cells, programmed cell death, response to UV/DNA damage repair/Fanconi anemia, cell cycle, transcriptional regulation, transcriptional activity, and transport/trafficking.

Six examples of smaller network modules identified as significant and biologically relevant are shown in figure 3; these include modules related to wound healing (associated with cancer invasion and progression to new sites), immune function (associated with stifling the body's ability to fight the cancer, mitochondrial function (associated with increased energy produc-

Table 4. Null subnetwork analysis.

| No. nodes | No. null subnetworks | Expected false positive subnets per dataset | Min no. subnets per dataset | Max <i>FDR</i> |
|-----------|----------------------|---|-----------------------------|--------------------|
| 3 | 40124 | 4.0 | 4 | 1 |
| 4 | 3392 | 0.34 | 1 | 0.34 |
| 5 | 365 | 0.037 | 1 | 0.037 |
| 6 | 48 | 0.0048 | 1 | 0.0048 |
| 7 | 4 | 4×10^{-4} | 1 | 4×10^{-4} |
| 8 | 1 | 1×10^{-4} | 1 | 1×10^{-4} |

10^4 iterations of null subnetworks were generated, by the same subnetwork identification method as used for the real data sets, but based on *p*-values randomly sampled from a uniform distribution. The table shows the number of subnetworks of each size which were declared as significant by the subnetwork identification method based on these null *p*-values, out of the 10^4 iterations. The table also shows the minimum number of subnetworks of each size detected in any of the real data sets (see table 3), and corresponding conservative estimates of the *FDR*, defined as the number of false positives divided by the number of discoveries, for each size of subnetwork.

doi:10.1371/journal.pone.0084573.t004

tion required for cancer proliferation) and MAP-kinase signalling (associated with regulation of cell proliferation). Summaries of the genes/nodes which appear in these network modules, and of the respective significantly enriched gene sets, appear in tables 6 and 7 (wound healing), tables 8 and 9 (immune), table S1 (mitochondrial), table S2 (MAP-kinase), and tables S3 and S4 (largest biologically significant subnetworks found in the BLCA and BRCA datasets, respectively).

Importantly, the network interactions in the wound healing module predominantly show an increase in network interaction co-ordinatedness with worse disease prognosis, indicating a tendency towards co-ordinated behaviour of these genes in support of metastatic processes. Conversely, the network interactions in the immune subnetwork module predominantly show a decrease in network interaction co-ordinatedness with worsening disease prognosis, suggesting a degradation of the body's own defences against the tumour. Hence, the DNA methylation network correlation measure, as a surrogate measure of more general interactive behaviour of genes, reflects increases and decreases in interactive behaviour in subnetwork modules which would be expected according to their biological function and role in disease.

The genes which comprise the wound healing module, and an outline of their biological roles, are as follows. ELANE is neutrophil elastase; it is secreted by neutrophils and macrophages

during inflammation, and destroys bacteria and host tissue [15]. KNG1 is kininogen 1, which uses alternative splicing to generate two different proteins, including HMWK which is important for coagulation of blood [16]. SERPINE1 encodes the serpin peptidase inhibitor, which plays a key role in the inhibition of fibrinolysis (the physiological breakdown of blood clots) [17]. F2R is proteinase-activated receptor 1, which is involved in the regulation of thrombotic response (clotting in blood vessels) [18]. F5 is factor five, a protein of the coagulation system; its deficiency leads to predisposition for haemorrhage [19]. CSF3 is granulocyte colony-stimulating factor, which promotes the differentiation and proliferation of blood cells [20]. ITGAM is integrin alpha M, which mediates inflammation by regulating leukocyte adhesion and migration [21]. THY1 is cluster of differentiation 90, which amongst other functions has a role in cell adhesion and migration [22].

The genes which comprise the immune module, and an outline of their biological roles, are as follows. HLA-A is a human leukocyte antigen (HLA); HLA constitute a large subset of the major histocompatibility complex (MHC, which mediates the interaction of immune system white blood cells) [23]. ITGAV is the vitronectin receptor integrin (integrins mediate attachment between a cell and its surroundings); vitronectin is found in serum and the extracellular matrix (ECM) and has been implicated in tumour malignancy [24]. SDC4 is syndecan 4, which interacts with ECM, anticoagulants, and growth-factors, and regulates the actin cytoskeleton, cell adhesion, and cell migration [25]. SDCBP is syndecan binding protein, which is thought to function as an adaptor protein, coupling the important developmental/pluripotency transcription factor SOX4 to the interleukin-5 receptor (which stimulates immune B-cell growth) [26]. CD247 encodes a component of the zeta-chain, which is part of the immune T-cell surface antigen receptor (TCR), which serves antigen recognition and signalling functions [27]. TMOD2 is a tropomodulin specific to neurons; tropomodulins cap the ends of actin filaments [28]. TAP1 is 'transporter associated with antigen processing, involved with transporting molecules across extra and intra cellular membranes, associated with the MHC [29]. HLA-F is another human leukocyte antigen (component of the MHC). ZAP-70 is zeta-chain-associated protein kinase 70, another component of the TCR [30]. EOMES is comesodermin, which encodes a transcription factor which is thought to be necessary for the differentiation of effector CD8+ T cells [31]. AP1G1 is AP-1 complex subunit gamma-1, which has a role in promoting the formation of clathrin-

Table 5. Directionality of significant network edges.

| Data set | Prop. <i>HR</i> >1 |
|----------|--------------------|
| BLCA | 0.32 |
| BRCA | 0.46 |
| HNSC | 0.47 |
| KIRC | 0.82 |
| LUAD | 0.66 |
| LUSC | 0.66 |
| UCEC | 0.37 |

The numbers in the second column indicate the proportion of network edges (i.e., pairs of genes) which increase (rather than decrease) their 'network interaction co-ordinatedness' for worse disease prognosis (i.e., the DNAm network correlation measure increases for shorter typical patient survival time, *HR* > 1).

doi:10.1371/journal.pone.0084573.t005

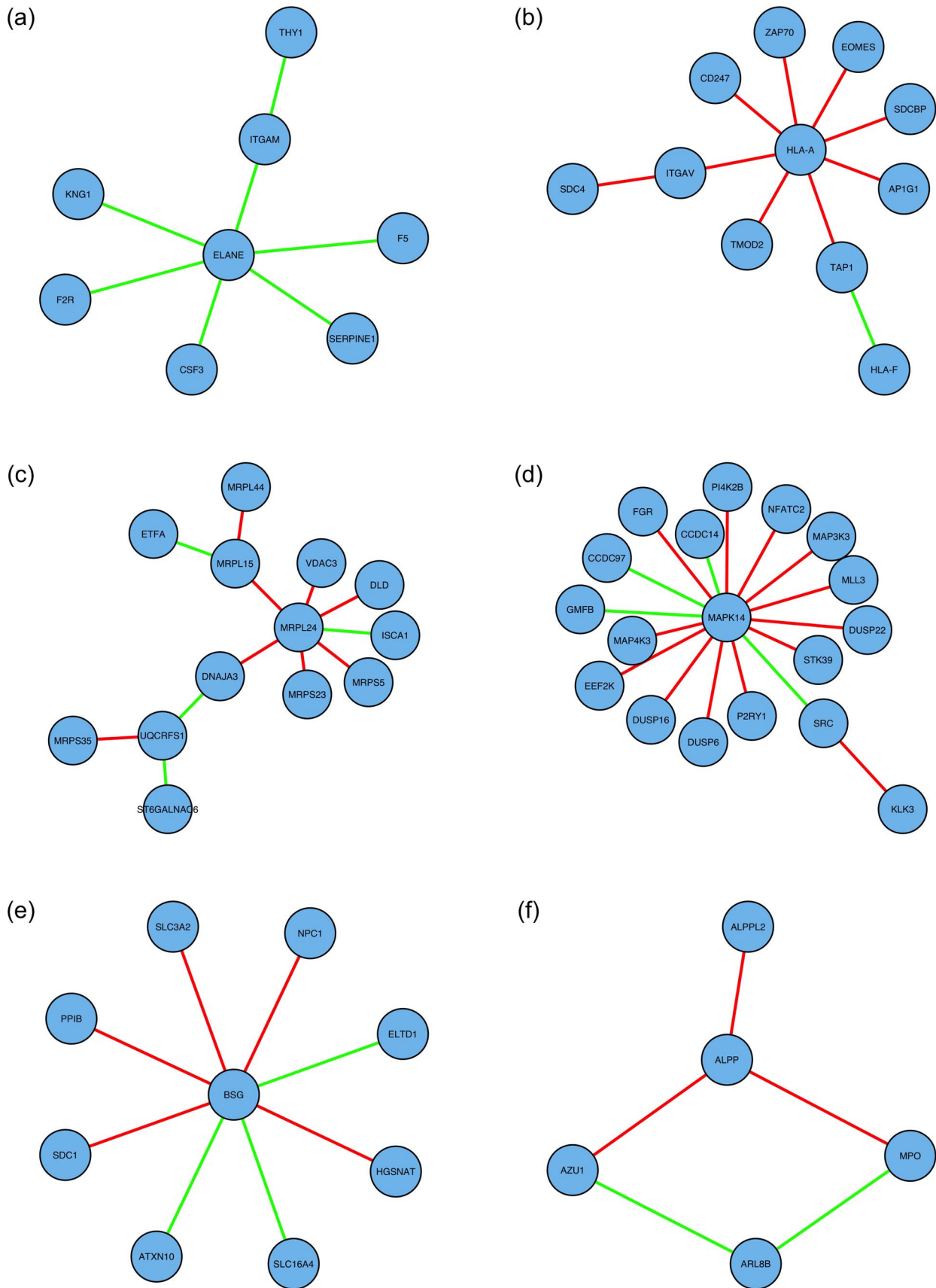


Figure 3. Smaller significant network modules: network diagrams. Network edges displayed in green and red indicate positive and negative hazard ratios, respectively, for the DNAm network correlation measure corresponding to that interaction; these correspond, respectively, to an

increase and decrease in ‘network interaction co-ordinatedness’ for worse disease prognosis. (a) Wound healing module (KIRC). (b) Immune module (UCEC). (c) Mitochondrial module (LUAD). (d) MAP-kinase module (LUSC). (e) Largest biologically significant subnetwork in the BLCA data set. (f) Largest biologically significant subnetwork in the BRCA data set. Further details about the corresponding network nodes (genes) and significantly enriched gene sets appear in tables 6–9 and S1–4. doi:10.1371/journal.pone.0084573.g003

coated pits and vesicles, which are used to transport molecules within and between cells [32].

Larger Significant Subnetworks

In each of two data sets, KIRC and LUAD, a larger significant subnetwork was also found (with 770 and 373 nodes respectively), and these are shown in figure 4; the higher density of nodes in the case of the KIRC large subnetwork is clearly seen in this figure. Both these large subnetworks were found to be biologically relevant, with 474 and 156 gene sets respectively found as significant by GSEA ($q < 0.05$). Degree distributions on a linear, and on a log-log scale, are shown in figure 5; there is power-law type behaviour in both cases for degree in the range 2 to 8 (linear model lines estimating the logarithm of the degree distribution, with corresponding slope estimates, are shown in the figure).

Considering the p -value histograms in figure 2, there are many more significant p -values for KIRC and LUAD than the other data sets, as can be seen by the height of the histogram bars closest to $p=0$, and correspondingly more significant network edges for these data sets. This may be why these data sets are the only ones for which such large subnetworks are found. Most of the data sets considered in this study have small sample sizes, particularly with respect to the number of events, and hence relatively low statistical power. If these methods were applied to larger data sets, larger subnetworks such as these might be able to be found for other cancer types. The degree density also decreases less as degree increases in the case of KIRC (figure 5 (b), slope = -1.8) than in the case of LUAD (figure 5 (b), slope = -2.6). This is as might be expected given that there are more significant network edges in the case of KIRC than LUAD (figure 2). This has the implication that LUAD shows fewer nodes of very high numbers of connections, so called ‘hubs’ (see also tables S5 and S6). The presence of ‘hubs’ is related to the probability of network failure. If a few nodes control the connectivity of the whole network, then their elimination will make the network fail. If the degree distribution is more even, and thus the slope less steep, then the network may be more resilient to failure. The slope is therefore an important characteristic of the network.

One feature of interest in relation to these two larger significant subnetworks is that they contain a high proportion of pairs of

genes (i.e., network edges) which increase their ‘network interaction co-ordinatedness’, the worse the prognosis of the cancer. In fact, this is a characteristic of the KIRC and LUAD data sets particularly, although not of all the data sets (table 5). This could be another reason why such large subnetworks are found for these data sets. Whereas interactions which correspond to a decrease in interactive behaviour with disease progression might logically correspond to fragmented, smaller motifs and modules, interactions which correspond to an increase in interactive behaviour with disease progression might be expected to coalesce to form larger subnetworks, with a tendency to act more autonomously.

Details about the genes/nodes in the top 5% of the degree distribution (as a summary of the most significant nodes) and the 25 most significantly enriched gene sets are shown in table S5 (KIRC) and table S6 (LUAD). It is particularly noticeable that there is enrichment by the genes in the significant large subnetworks of many genes sets associated with transcriptional and translational processes, and perhaps the most interesting of these in the context of DNAm relate to splicing. For example, the splicing factor gene SF3B4 is the node with the second highest degree in the KIRC large subnetwork (table S5 (a)), and the KEGG spliceosome gene set is very significantly enriched by the nodes of the KIRC large subnetwork, $OR = 5.7$ (95% C.I. 3.5–9.2), FDR-adjusted $p = 8.7 \times 10^{-9}$ (Fishers exact test), table S5 (b). DNA methylation has been suggested to have an important association with alternative splicing [33], although how this might work is poorly understood. It is very interesting that the largest significant subnetworks identified by this method appear to be involved in these processes, amongst other forms of gene regulatory behaviour, and more generally cancer-related processes.

Discussion

A DNA methylation (DNAm) measure of network correlation has been developed, as a measure of ‘network interaction co-ordinatedness’, between pairs of genes, in terms of their DNAm profiles. This measure has been shown to be highly associated with the correlation of gene expression measurements (at the mRNA level) from the same pairs of genes in five independent data sets

Table 6. Wound-healing module: gene/node details.

| Gene/node | Degree | Chr | Gene info |
|-----------|--------|-----|---|
| ELANE | 6 | 19 | elastase, neutrophil expressed |
| ITGAM | 2 | 16 | integrin, alpha M (complement component 3 receptor 3 subunit) |
| CSF3 | 1 | 17 | colony stimulating factor 3 (granulocyte) |
| F2R | 1 | 5 | coagulation factor II (thrombin) receptor |
| F5 | 1 | 1 | coagulation factor V (proaccelerin, labile factor) |
| KNG1 | 1 | 3 | kininogen 1 |
| SERPINE1 | 1 | 7 | serpin peptidase inhibitor, clade E (nexin, plasminogen activator inhibitor type 1), member 1 |
| THY1 | 1 | 11 | Thy-1 cell surface antigen |

Gene/node details for the wound healing module found as significant in the KIRC data set.

doi:10.1371/journal.pone.0084573.t006

Table 7. Wound-healing module: significantly enriched gene sets.

| Gene set | OR (95% C.I.) | q-val |
|---|---------------|---------|
| BLOOD_COAGULATION | 290 (52–1600) | 5.3e-05 |
| COAGULATION | 290 (52–1600) | 5.3e-05 |
| HEMOSTASIS | 250 (46–1500) | 5.7e-05 |
| WOUND_HEALING | 230 (42–1300) | 5.9e-05 |
| REGULATION_OF_BODY_FLUID_LEVELS | 210 (37–1100) | 7e-05 |
| KEGG_COMPLEMENT_AND_COAGULATION_CASCADES | 200 (36–1100) | 7e-05 |
| BIOCARTA_INTRINSIC_PATHWAY | 450 (63–2600) | 0.00023 |
| NEGATIVE_REGULATION_OF_MULTICELLULAR_ORGANISMAL_PROCESS | 320 (45–1800) | 0.00054 |
| WANG_ESOPHAGUS_CANCER_VS_NORMAL_UP | 100 (19–580) | 0.00057 |
| PID_INTEGRIN2_PATHWAY | 230 (34–1300) | 0.001 |
| REGULATION_OF_BIOLOGICAL_QUALITY | 50 (9.7–320) | 0.0014 |
| RESPONSE_TO_WOUNDING | 69 (13–380) | 0.0019 |
| PID_UPA_UPAR_PATHWAY | 170 (25–940) | 0.0019 |
| REACTOME_HEMOSTASIS | 41 (7.9–260) | 0.003 |
| REACTOME_PLATELET_ACTIVATION_SIGNALING_AND_AGGREGATION | 54 (9.9–290) | 0.0044 |
| BIOCARTA_FIBRINOLYSIS_PATHWAY | 680 (53–8200) | 0.006 |
| RESPONSE_TO_EXTERNAL_STIMULUS | 42 (7.8–230) | 0.0092 |
| REACTOME_RESPONSE_TO_ELEVATED_PLATELET_CYTOSOLIC_CA2_ | 86 (13–450) | 0.0092 |
| BIOCARTA_GRANULOCYTES_PATHWAY | 460 (38–4100) | 0.0094 |
| RECEPTOR_BINDING | 35 (6.6–190) | 0.016 |
| BIOCARTA_EXTRINSIC_PATHWAY | 310 (27–2200) | 0.017 |
| REGULATION_OF_MULTICELLULAR_ORGANISMAL_PROCESS | 52 (7.9–270) | 0.032 |
| RPS14_DN.V1_UP | 47 (7.2–250) | 0.041 |

Significantly enriched gene sets, for the wound healing module found as significant in the KIRC data set. Q-values indicate significance of enrichment in the corresponding gene set by the genes in this module, calculated according to a one-sided Fisher’s exact test. Further details about these gene sets can be found from the website of the Broad Institute Molecular Signatures Database (<http://www.broadinstitute.org>). doi:10.1371/journal.pone.0084573.t007

from different cancer types; i.e., the DNAm network correlation measure reflects well co-regulatory behaviour relating to gene expression. This measure has been tested for association with patient overall survival outcome independent of known clinical prognostic features in nine independent data sets corresponding to different cancer types; independent association with survival

outcome was found for this measure in seven out of nine of these data sets, with strong association in five of these, which are Breast Invasive Carcinoma (BRCA), Kidney Renal Clear Cell Carcinoma (KIRC), Lung Adenocarcinoma (LUAD), Lung Squamous Cell Carcinoma (LUSC), and Uterine Corpus Endometrioid Carcinoma (UCEC). For each of these data sets (cancer types),

Table 8. Immune module: gene/node details.

| Gene/node | Degree | Chr | Gene info |
|-----------|--------|-----|---|
| HLA-A | 8 | 6 | major histocompatibility complex, class I, A |
| ITGAV | 2 | 2 | integrin, alpha V |
| TAP1 | 2 | 6 | transporter 1, ATP-binding cassette, sub-family B (MDR/TAP) |
| AP1G1 | 1 | 16 | adaptor-related protein complex 1, gamma 1 subunit |
| CD247 | 1 | 1 | CD247 molecule |
| EOMES | 1 | 3 | eomesodermin |
| SDCBP | 1 | 8 | syndecan binding protein (syntenin) |
| TMOD2 | 1 | 15 | tropomodulin 2 (neuronal) |
| ZAP70 | 1 | 2 | zeta-chain (TCR) associated protein kinase 70 kDa |
| HLA-F | 1 | 6 | major histocompatibility complex, class I, F |
| SDC4 | 1 | 20 | syndecan 4 |

Gene/node details for the immune module found as significant in the UCEC data set. doi:10.1371/journal.pone.0084573.t008

Table 9. Immune module: significantly enriched gene sets.

| Gene set | OR (95% C.I.) | q-val |
|---|---------------|--------|
| REACTOME_ADAPTIVE_IMMUNE_SYSTEM | 37 (9.3–170) | 0.001 |
| REACTOME_ANTIGEN_PROCESSING_CROSS_PRESENTATION | 97 (20–390) | 0.0019 |
| REACTOME_ANTIGEN_PRESENTATION_FOLDING_ASSEMBLY_AND_PEPTIDE_LOADING_OF_CLASS_I_MHC | 210 (33–980) | 0.0036 |
| REACTOME_THE_ROLE_OF_NEF_IN_HIV1_REPLICATION_AND_DISEASE_PATHOGENESIS | 140 (23–670) | 0.006 |
| REACTOME_IMMUNE_SYSTEM | 22 (5.5–100) | 0.006 |
| KEGG_CELL_ADHESION_MOLECULES_CAMS | 52 (11–210) | 0.0069 |
| GNF2_HLA-C | 110 (17–480) | 0.0094 |
| GNF2_INPP5D | 100 (17–460) | 0.0094 |
| GNF2_ITGAL | 100 (16–440) | 0.0094 |
| REACTOME_IMMUNOREGULATORY_INTERACTIONS_BETWEEN_A_LYMPHOID_AND_A_NON_LYMPHOID_CELL | 89 (15–390) | 0.012 |
| RECEPTOR_COMPLEX | 76 (13–330) | 0.013 |
| GNF2_CD53 | 80 (13–350) | 0.013 |
| KEGG_ANTIGEN_PROCESSING_AND_PRESENTATION | 76 (13–330) | 0.013 |
| PID_CD8TCRDOWNSTREAMPATHWAY | 80 (13–350) | 0.013 |
| PID_CD8TCRPATHWAY | 71 (12–310) | 0.014 |
| REACTOME_ER_PHAGOSOME_PATHWAY | 71 (12–310) | 0.014 |
| REACTOME_ENDOSOMAL_VACUOLAR_PATHWAY | 370 (32–2500) | 0.015 |
| DER_IFN_ALPHA_RESPONSE_UP | 66 (11–290) | 0.015 |
| PID_IL12_2PATHWAY | 65 (11–280) | 0.015 |
| BIOCARTA_TCRA_PATHWAY | 310 (27–2200) | 0.015 |
| REACTOME_NEF_MEDIATED_DOWNREGULATION_OF_MHC_CLASS_I_COMPLEX_CELL_SURFACE_EXPRESSION | 310 (27–2200) | 0.015 |
| REACTOME_TRANSLOCATION_OF_ZAP_70_TO_IMMUNOLOGICAL_SYNAPSE | 310 (27–2200) | 0.015 |
| DER_IFN_GAMMA_RESPONSE_UP | 61 (10–270) | 0.015 |
| BIOCARTA_CTL_PATHWAY | 270 (24–1600) | 0.018 |
| MODULE_293 | 270 (24–1600) | 0.018 |
| REACTOME_CLASS_I_MHC_MEDIATED_ANTIGEN_PROCESSING_PRESENTATION | 27 (5.8–110) | 0.018 |
| IMMUNOLOGICAL_SYNAPSE | 230 (21–1400) | 0.021 |
| MODULE_143 | 210 (19–1200) | 0.025 |
| GNF2_MATK | 140 (14–820) | 0.043 |
| KEGG_NATURAL_KILLER_CELL_MEDIATED_CYTOTOXICITY | 38 (6.4–160) | 0.043 |
| SENGUPTA_EBNA1_ANTICORRELATED | 38 (6.4–160) | 0.043 |
| GNF2_ZAP70 | 130 (13–740) | 0.045 |
| BIOCARTA_CSK_PATHWAY | 130 (13–740) | 0.045 |

Significantly enriched gene sets, for the immune module found as significant in the UCEC data set. Q-values indicate significance of enrichment in the corresponding gene set by the genes in this module, calculated according to a one-sided Fisher's exact test. Further details about these gene sets can be found from the website of the Broad Institute Molecular Signatures Database (<http://www.broadinstitute.org>). doi:10.1371/journal.pone.0084573.t009

significant subnetworks, modules, and motifs have been found, with the associated false discovery rate shown to be well-controlled for those with at least 5 nodes (genes). In many cases, these significant subnetwork modules are shown to have strong correlation with groups of genes previously found to be biologically relevant, in the context of cancer biology.

The smaller significant subnetwork modules identified in relation to previous knowledge of cancer biology include ones identified with wound healing (associated with cancer invasion and progression to new sites), mitochondrial function (associated with increased energy production required for cancer proliferation), immune function (associated with stifling the body's ability to fight the cancer), and MAP-kinase signalling (associated with regulation of cell proliferation). The wound healing module interactions show an increase in network co-ordinatedness with worsening disease

prognosis, indicating a tendency towards a re-wiring of this module in support of metastatic processes. The immune module interactions show a decrease in network co-ordinatedness with worsening disease prognosis, suggesting a degradation of the body's own defences against the tumour. Larger significant subnetworks found are associated, amongst other things, with functions related to DNA transcription, translation and regulation. These functions notably include those related to splicing, which is of particular interest in relation to current DNAm research.

Wound healing is an example of a biological function which behaves aberrantly in the context of cancer biology, highlighted in a recent paper [34] which fundamentally shifts the paradigm of oncogenesis. Those authors suggest that tumourigenic processes are actually a regression to archaic metazoan phenotypic characteristics normally suppressed in healthy tissue, which

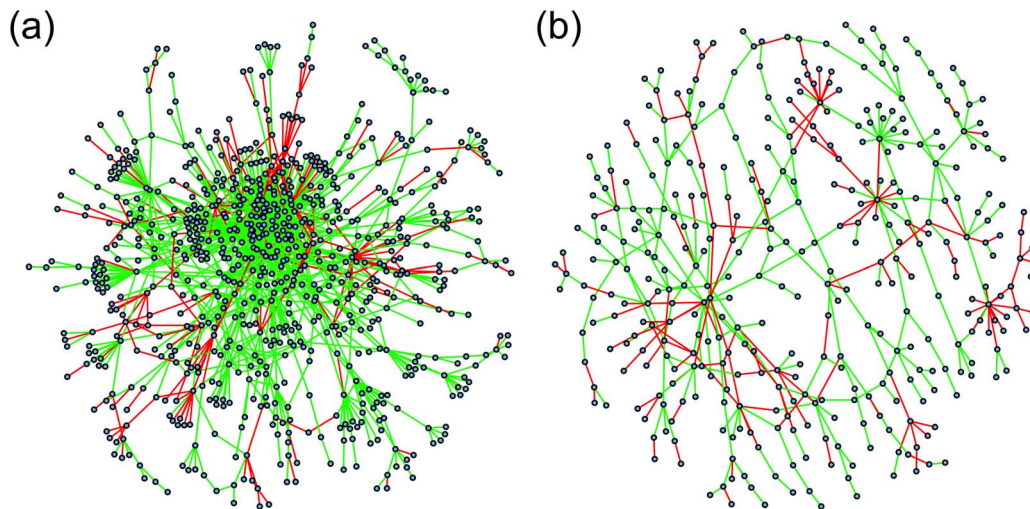


Figure 4. Larger significant subnetworks: network diagrams. Network edges displayed in green and red indicate positive and negative hazard ratios, respectively, for the DNAm network correlation measure corresponding to that interaction; these correspond, respectively, to an increase and decrease in ‘network interaction co-ordinatedness’ for worse disease prognosis. (a) the KIRC large subnetwork. (b) the LUAD large subnetwork. Further details about the corresponding network nodes (genes) for the top 5% of the degree distribution and top 25 significantly enriched gene sets appear in tables S5–6.

doi:10.1371/journal.pone.0084573.g004

correspond to groups of cells behaving more autonomously. The key point in this metazoan model is that, whereas the conventional model of tumorigenesis holds that proliferative characteristics acquired by cancers occur as a result of random genetic and epigenetic mutation, these archaic metazoan characteristics are present in humans all along, but lie dormant until they are released in cancer. The data considered in this study does not allow this point to be addressed directly, but intuitively it seems that our findings fit well into this new metazoan oncogenic paradigm.

The quality of the presented study depends on the availability of clinical data. However, information is missing for many samples for several clinical covariates. Also, for a number of clinical covariates, the large majority of the samples are in the same category for that covariate. It should therefore be expected that this analysis will not have fully taken account of some clinical covariates. Further, the clinical information considered does not include descriptions of applied therapies. For these reasons, more detailed analyses relating to specific cancers should be expected to be necessary for the further development of clinical biomarkers based on the methods developed here.

While the data sets considered in this study do not contain enough events to train a predictive model, bigger data sets would allow such predictive prognostic models to be defined using these methods, leading to novel independent DNAm-based disease prognostic biomarkers. Such biomarkers would be based on DNA rather than RNA, and would be ideal for further investigation and development using current state-the-art and future research findings from the rapidly advancing field of network science.

Methods and Models

Data Download and Preprocessing

DNA methylation (DNAm) data, collected via the Illumina Infinium HumanMethylation450 platform, were downloaded from The Cancer Genome Atlas (TCGA) project [9–11] at level 3. These data were obtained for nine different tumour types, as follows: Bladder Urothelial Carcinoma (BLCA), Breast Invasive Carcinoma (BRCA), Colon Adenocarcinoma (COAD), Head and

Neck Squamous Cell Carcinoma (HNSC), Kidney Renal Clear Cell Carcinoma (KIRC), Liver (LIHC), Lung Adenocarcinoma (LUAD), Lung Squamous Cell Carcinoma (LUSC), and Uterine Corpus Endometrioid Carcinoma (UCEC).

These data were pre-processed by first removing probes with non-unique mappings and which map to SNPs (as identified in the TCGA level 3 data); probes mapping to sex chromosomes were also removed; in total 98384 probes were removed in this way from all data sets. After removal of these probes, 270985 probes with known gene annotations remained. Individually for each data set, probes were then removed if they had less than 95% coverage across samples; probe values were also replaced if they had corresponding detection p -value greater than 5%, by KNN (k nearest neighbour) imputation ($k=5$). The loci of analysed CpGs were mapped to genes based on annotation information for the Illumina Infinium platform obtained from the R [35]/Bioconductor [36] package ‘IlluminaHumanMethylation450 k’. The data were also checked for batch effects by hierarchical clustering and correlation of the significant principle components with phenotype and batch: no significant batch effects (which would warrant further correction) were found.

A list of pairs of genes, each pair corresponding to a known biochemical interaction in humans, was downloaded from <http://www.pathwaycommons.org>, and was used as a canonical human interactome map in the subsequent analysis. In this network model, each pair of genes defines a network edge (422481 edges in total), with individual genes represented by network nodes (12726 nodes in total).

For each data set/cancer type, clinical information was also downloaded, for the variables overall survival status (alive or not), overall survival time (i.e., time to last follow up or time to death), as well as several clinical covariates for each data set, such as age, disease stage (I–IV), disease grade (1–3), and residual disease status (present or not). All survival analyses were carried out using the R [35] package ‘survival’.

For five of the cancer types (BRCA, COAD, KIRC, LUSC and UCEC), gene expression data were also downloaded from TCGA at level 3. These data were quantile-normalised.

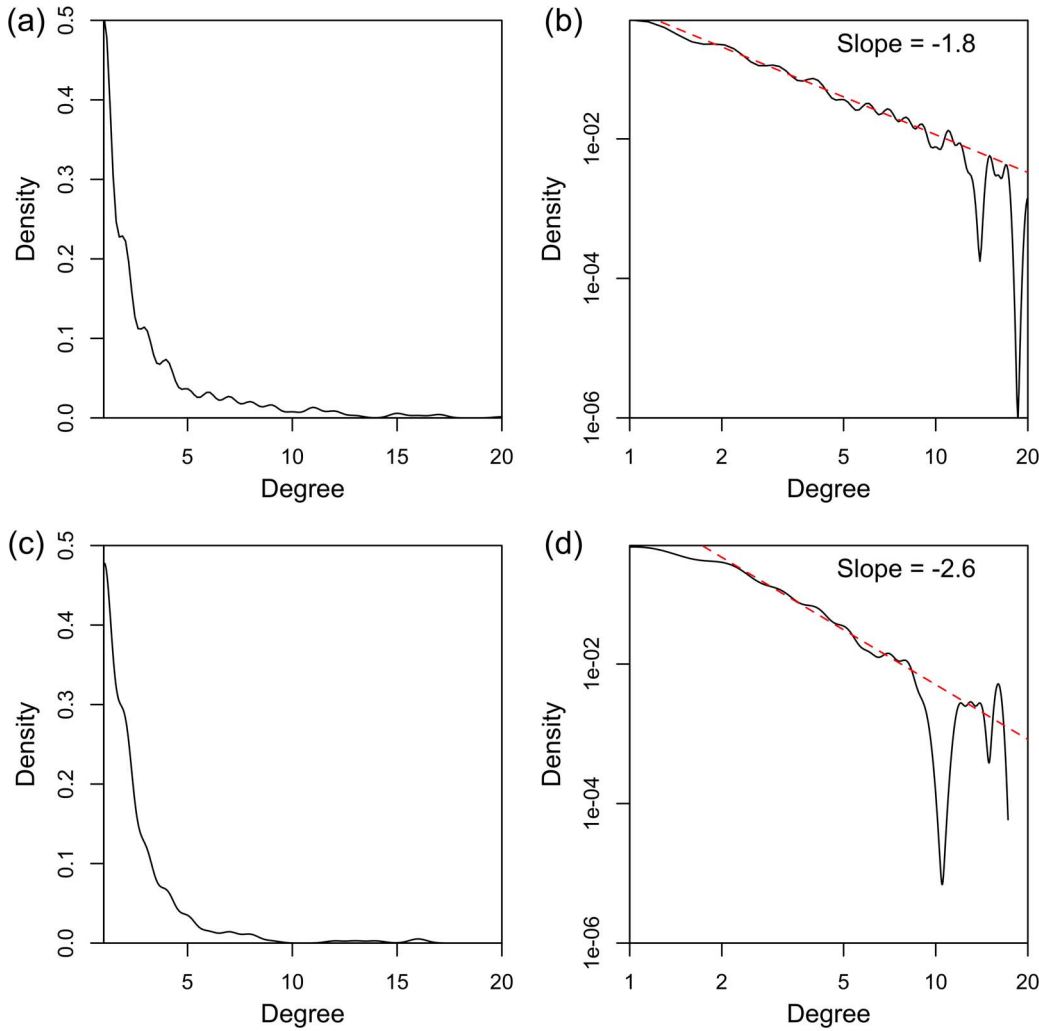


Figure 5. Larger significant subnetworks: degree distributions. Degree distributions (kernel-smoothed) on linear and log scales, for (a), (b) KIRC large subnetwork, and (c), (d) LUAD large subnetwork. Dashed red lines on the log-log plots display the power-law linear model line of best fit, estimated from the nodes with degree in the range 2 to 8, with the corresponding slope value (i.e., power law exponential coefficient) displayed above.

doi:10.1371/journal.pone.0084573.g005

DNA Methylation Network Correlation Measure

Definitions

Canonical correlation analysis (CCA) [8] seeks to find the vectors a and b , in the p and q dimensional spaces of variables $\mathbf{X} = (x_1, x_2, \dots, x_p)'$ and $\mathbf{Y} = (y_1, y_2, \dots, y_q)'$ respectively, which maximise the correlation $\rho = \text{cor}(\mathbf{a}'\mathbf{X}, \mathbf{b}'\mathbf{Y})$, defined according to equation 1,

$$\rho = \frac{\mathbf{a}'\Sigma_{\mathbf{X}\mathbf{Y}}\mathbf{b}}{\sqrt{\mathbf{a}'\Sigma_{\mathbf{X}\mathbf{X}}\mathbf{a}}\sqrt{\mathbf{b}'\Sigma_{\mathbf{Y}\mathbf{Y}}\mathbf{b}}} \quad (1)$$

where $\Sigma_{\mathbf{X}\mathbf{X}} = \mathbb{E}[(\mathbf{X} - \mu_{\mathbf{X}})(\mathbf{X} - \mu_{\mathbf{X}})']$ and $\Sigma_{\mathbf{Y}\mathbf{Y}} = \mathbb{E}[(\mathbf{Y} - \mu_{\mathbf{Y}})(\mathbf{Y} - \mu_{\mathbf{Y}})']$ are the covariance matrices of \mathbf{X} and \mathbf{Y} respectively, and $\Sigma_{\mathbf{X}\mathbf{Y}} = \mathbb{E}[(\mathbf{X} - \mu_{\mathbf{X}})(\mathbf{Y} - \mu_{\mathbf{Y}})']$ is the cross-covariance matrix of \mathbf{X} and \mathbf{Y} .

Two genes X and Y , which are joined by a network edge in the interactome map (i.e., these genes or their products participate in some canonical biochemical interaction), have corresponding methylation profiles which are measured for sample/patient j at p and q CpGs (loci) respectively along these genes. Denoting these

measurements by the variables x_1, \dots, x_p and y_1, \dots, y_q for genes X and Y respectively, the DNA methylation profiles for these genes, for patient j , can be represented by the vectors $\mathbf{x}(j)$ and $\mathbf{y}(j)$, which have p and q entries respectively. A measure of DNAm network correlation $\rho_{xy}(j)$, of the methylation profiles of genes X and Y for sample j , can then be defined by analogy with equation 1, according to equation 2,

$$\hat{\rho}_{xy}(j) = \frac{\mathbf{x}(j)^T \hat{\Sigma}_{\mathbf{X}\mathbf{Y}}^{(h)} \mathbf{y}(j)}{\sqrt{\mathbf{x}(j)^T \hat{\Sigma}_{\mathbf{X}\mathbf{X}}^{(h)} \mathbf{x}(j)} \sqrt{\mathbf{y}(j)^T \hat{\Sigma}_{\mathbf{Y}\mathbf{Y}}^{(h)} \mathbf{y}(j)}} \quad (2)$$

where $\hat{\Sigma}_{\mathbf{X}\mathbf{X}}^{(h)}$, $\hat{\Sigma}_{\mathbf{Y}\mathbf{Y}}^{(h)}$ and $\hat{\Sigma}_{\mathbf{X}\mathbf{Y}}^{(h)}$ are estimated from healthy rather than cancer samples in the methylation data set, according to equations 3–5,

$$\hat{\Sigma}_{\mathbf{X}\mathbf{X}}^{(h)} = \frac{1}{n_h} \sum_{j \in \text{healthy}} (\mathbf{x}(j) - \hat{\mu}_{\mathbf{X}}^{(h)}) (\mathbf{x}(j) - \hat{\mu}_{\mathbf{X}}^{(h)})^T \quad (3)$$

$$\hat{\Sigma}_{YY}^{(h)} = \frac{1}{n_h} \sum_{j \in \text{healthy}} (\mathbf{y}(j) - \hat{\mu}_Y^{(h)}) (\mathbf{y}(j) - \hat{\mu}_Y^{(h)})^T \quad (4)$$

$$\hat{\Sigma}_{XY}^{(h)} = \frac{1}{n_h} \sum_{j \in \text{healthy}} (\mathbf{x}(j) - \hat{\mu}_X^{(h)}) (\mathbf{y}(j) - \hat{\mu}_Y^{(h)})^T \quad (5)$$

where

$$\hat{\mu}_X^{(h)} = \frac{1}{n_h} \sum_{j \in \text{healthy}} \mathbf{x}(j)$$

and

$$\hat{\mu}_Y^{(h)} = \frac{1}{n_h} \sum_{j \in \text{healthy}} \mathbf{y}(j)$$

and n_h is the number of healthy samples in the data set.

Selection of Significant Clinical Covariates

If a clinical covariate (e.g., age, disease stage and grade, or presence of residual disease) associates significantly with the patient outcome of interest (here, overall survival time) and also with the predictors of interest (here, the DNAm network correlation measure), then any association between the predictors and outcome of interest might be due only to the variation of the clinical covariate(s). In order to develop novel DNA methylation biomarkers which are independent of known prognostic clinical features, the statistical tests of association with patient survival outcome are adjusted here for the clinical covariates which also associate significantly with patient survival outcome.

For each data set (corresponding to a particular cancer type), the available clinical covariates were tested one by one for association with overall survival outcome, by fitting a Cox model. For each data set, the covariates for which this association corresponded to $p < 0.1$ were then considered further, in a multivariate Cox model. Because clinical covariates may be measuring correlated physiological quantities (e.g., height and weight, or in some cases disease stage and grade), it is only necessary to adjust for a clinical covariate in the subsequent DNAm survival analysis if that clinical covariate associates significantly with survival after adjustment for the other clinical covariates. Therefore, the clinical covariates found to be significant in the first stage (by testing their association one by one with overall survival outcome) were tested against each other in a multivariate Cox regression, and those which remained significant ($p < 0.1$) after adjustment for the other clinical covariates were then adjusted for in the subsequent DNAm survival analysis.

For each data set, the clinical covariates which were considered are as follows, with those ultimately found to associate with overall survival ($p < 0.1$), and thus adjusted for in the DNAm survival analysis, shown in bold.

- **BLCA: stage**, age, grade, diagnosis subtype, anatomic organ subdivision, height, prior diagnosis, gender, tobacco history, weight.
- **BRCA: age, residual disease**, stage, gender, ER status, PR status.

- **COAD: age, stage, prior diagnosis, residual disease**, anatomic site, histology, polyps, lymphatic invasion, perineural invasion, gender, height, weight.
- **HNSC: residual disease, tobacco history**, age, stage, grade, prior diagnosis, pack years, lymph node presentation, gender.
- **KIRC: age, stage, prior diagnosis, residual disease**, grade, haemoglobin, platelet, lymph node, calcium, gender.
- **LHC: creatinine, prothrombin**, age, stage, grade, prior diagnosis, residual disease, prospective tissue collection, platelet, albumin, alpha fetoprotein, fibrosis, gender, height, weight.
- **LUAD: residual disease**, age, stage, tobacco history, prior diagnosis, gender.
- **LUSC: residual disease**, age, stage, tobacco history, gender.
- **UCEC: stage, residual disease**, age, grade, prior diagnosis, height, weight.

Supporting Information

Figure S1 p -value heatmaps, showing the association of the DNAm network correlation measure with patient overall survival outcome, for the BRCA data set. For the BRCA data set, for each network edge (DNAm network interaction correlation measure), the Cox regression p -value (adjusted for clinical covariates) of association with patient survival outcome is displayed according to the colour scale shown on the right. (a) p -values are calculated for every possible pair of genes of the 14800 available in this data set, with genes clustered along the margins of the plot using these p -values as a distance measure. (b) Null p -values are generated by sampling from a uniform distribution bounded on $[0,1]$ for every possible pair of genes, with genes similarly clustered along the margins. (c) and (e) p -values are calculated for the 8614 genes which appear in this data set and also in the pathway commons interactome map, for the 276136 interactions between pairs of these genes defined by this interactome map. Genes are similarly clustered along the margins of the plot according to p -value. (e) Shows a zoomed-in view of the top-left of (c). (d) and (f) are as (c) and (e), but based on null p -values randomly sampled from a uniform $(0,1)$ distribution, to demonstrate the structure present from the pathway commons interactome map, without the influence of the DNA methylation network interaction measure. Pearson correlation coefficients comparing values in these adjacency matrices as plotted, are as follows: (a) vs. (b), 0.0011; (c) vs. (d), 0.26; (e) vs. (f), 0.38.

(JPG)

Table S1 Mitochondrial module.

(PDF)

Table S2 MAP-kinase module.

(PDF)

Table S3 Largest biologically significant module, BLCA.

(PDF)

Table S4 Largest biologically significant module, BRCA.

(PDF)

Table S5 KIRC large subnetwork.

(PDF)

Table S6 LUAD large subnetwork.
(PDF)

Acknowledgments

We are very grateful to all specimen donors and research groups involved in providing the data used in this study via TCGA.

References

1. Feinberg A, Ohlsson R, Henikoff S (2006) The epigenetic progenitor origin of human cancer. *Nature reviews genetics* 7: 21–33.
2. Cooney CA (2007) Epigenetics-dna-based mirror of our environment? *Disease Markers* 23: 121–137.
3. Christensen BC, Houseman EA, Marsit CJ, Zheng S, Wrensch MR, et al. (2009) Aging and environmental exposures alter tissue-specific dna methylation dependent upon cpg island context. *PLoS genetics* 5: e1000602.
4. Bartlett TE, Zaikin A, Olhede SC, West J, Teschendorff AE, et al. (2013) Corruption of the intragene dna methylation architecture is a hallmark of cancer. *PLoS one* 8: e68285.
5. Barabási AL, Oltvai ZN (2004) Network biology: understanding the cell's functional organization. *Nature Reviews Genetics* 5: 101–113.
6. Taylor IW, Linding R, Warde-Farley D, Liu Y, Pesquita C, et al. (2009) Dynamic modularity in protein interaction networks predicts breast cancer outcome. *Nature biotechnology* 27: 199–204.
7. Jones P (2012) Functions of dna methylation: islands, start sites, gene bodies and beyond. *Nature Reviews Genetics* 13: 484–492.
8. Hotelling H (1936) Relations between two sets of variates. *Biometrika* 28: 321–377.
9. Hampton T (2006) Cancer genome atlas. *JAMA: The Journal of the American Medical Association* 296: 1958–1958.
10. Bonetta L (2006) Genome sequencing in the fast lane. *Nature Methods* 3: 141.
11. Collins F, Barker A (2007) Mapping the cancer genome. *Scientific American Magazine* 296: 50–57.
12. Leek J (2011) Asymptotic conditional singular value decomposition for high-dimensional genomic data. *Biometrics* 67: 344–352.
13. Benjamini Y, Hochberg Y (1995) Controlling the false discovery rate: a practical and powerful approach to multiple testing. *Journal of the Royal Statistical Society Series B (Methodological)* : 289–300.
14. Subramanian A, Tamayo P, Mootha V, Mukherjee S, Ebert B, et al. (2005) Gene set enrichment analysis: a knowledge-based approach for interpreting genome-wide expression profiles. *Proceedings of the National Academy of Sciences of the United States of America* 102: 15545.
15. Belaouaj A, Kim KS, Shapiro SD (2000) Degradation of outer membrane protein a in *Escherichia coli* killing by neutrophil elastase. *Science* 289: 1185–1187.
16. Sabater-Lleal M, Martinez-Perez A, Buil A, Folkersen L, Souto JC, et al. (2012) A genome-wide association study identifies *kn1g1* as a genetic determinant of plasma factor xi level and activated partial thromboplastin time. *Arteriosclerosis, thrombosis, and vascular biology* 32: 2008–2016.
17. Mimuro J (1991) Type 1 plasminogen activator inhibitor: its role in biological reactions. *Rinsho Ketsueki/The Japanese Journal of Clinical Hematology* 32: 487–489.
18. Coughlin SR, Vu TK, Hung D, Wheaton V (1992) Characterization of a functional thrombin receptor. issues and opportunities. *Journal of Clinical Investigation* 89: 351.
19. Owren PA (1947) Parahaemophilia: haemorrhagic diathesis due to absence of a previously unknown clotting factor. *The Lancet* 249: 446–448.
20. Lovejoy B, Cascio D, Eisenberg D (1993) Crystal structure of canine and bovine granulocyte-colony stimulating factor (g-csf). *Journal of molecular biology* 234: 640–653.
21. Solovjov D, Pluskota E, Plow E (2005) Distinct roles for the alpha and beta subunits in the functions of integrin alphabeta2. *Journal of biological chemistry* 280: 1336–1345.
22. Rege TA, Hagood JS (2006) Thy-1 as a regulator of cell-cell and cell-matrix interactions in axon regeneration, apoptosis, adhesion, migration, cancer, and fibrosis. *The FASEB journal* 20: 1045–1054.
23. Trägårdh L, Rask L, Wiman K, Fohlman J, Peterson PA (1980) Complete amino acid sequence of pooled papain-solubilized hla-a, -b, and -c antigens: relatedness to immunoglobulins and internal homologies. *Proceedings of the National Academy of Sciences* 77: 1129–1133.
24. Felding-Habermann B, Cheresh DA (1993) Vitronectin and its receptors. *Current opinion in cell biology* 5: 864–868.
25. Woods A, Couchman JR (1998) Syndecans: synergistic activators of cell adhesion. *Trends in cell biology* 8: 189–192.
26. Geijsen N, Uings IJ, Pals C, Armstrong J, McKinnon M, et al. (2001) Cytokine-specific transcriptional regulation through an *il-5* receptor interacting protein. *Science* 293: 1136–1138.
27. Weissman AM, Hou D, Orloff DG, Modi WS, Seunanez H, et al. (1988) Molecular cloning and chromosomal localization of the human t-cell receptor zeta chain: distinction from the molecular cd3 complex. *Proceedings of the National Academy of Sciences* 85: 9709–9713.
28. Cox PR, Siddique T, Zoghbi HY (2001) Genomic organization of tropomodulins 2 and 4 and unusual intergenic and intraexonic splicing of *yl-1* and tropomodulin 4. *BMC genomics* 2: 7.
29. Bahram S, Arnold D, Bresnahan M, Strominger JL, Spies T (1991) Two putative subunits of a peptide pump encoded in the human major histocompatibility complex class ii region. *Proceedings of the National Academy of Sciences* 88: 10094–10098.
30. Chan AC, Iwashima M, Turck CW, Weiss A (1992) Zap-70: a 70 kd protein-tyrosine kinase that associates with the tcr ζ chain. *Cell* 71: 649–662.
31. McLane LM, Banerjee PP, Cosma GL, Makedonas G, Wherry EJ, et al. (2013) Differential localization of t-bet and comes in cd8 t cell memory populations. *The Journal of Immunology* 190: 3207–3215.
32. Takatsu H, Sakurai M, Shin HW, Murakami K, Nakayama K (1998) Identification and characterization of novel clathrin adaptor-related proteins. *Journal of Biological Chemistry* 273: 24693–24700.
33. Guo JU, Ma DK, Mo H, Ball MP, Jang MH, et al. (2011) Neuronal activity modifies the dna methylation landscape in the adult brain. *Nature neuroscience* 14: 1345–1351.
34. Davies P, Lineveaver C (2011) Cancer tumors as metazoa 1.0: tapping genes of ancient ancestors. *Physical biology* 8: 015001.
35. R Core Team (2013) R: A Language and Environment for Statistical Computing. R Foundation for Statistical Computing, Vienna, Austria. URL <http://www.R-project.org>. Accessed 2013 September 17.
36. Gentleman RC, Carey VJ, Bates DM, Bolstad B, Dettling M, et al. (2004) Bioconductor: Open software development for computational biology and bioinformatics. *Genome Biology* 5: R80.

Author Contributions

Conceived and designed the experiments: TEB SCO AZ. Performed the experiments: TEB. Analyzed the data: TEB. Contributed reagents/materials/analysis tools: TEB SCO AZ. Wrote the paper: TEB SCO AZ.